

Generation-Step-Aware Framework for Cross-Modal Representation and Control in Multilingual Speech–Text Models

Toshiki Nakai¹ Varsha Suresh¹ Vera Demberg^{1,2}

¹Saarland University

²Max Planck Institute for Informatics, Saarland Informatics Campus
toshiki3738@gmail.com

Abstract

Multilingual speech–text models rely on cross-modal language alignment to transfer knowledge between speech and text, but it remains unclear whether this reflects shared computation for the same language or modality-specific processing. We introduce a generation-step-aware framework for evaluating cross-modal computation that (i) identifies language-selective neurons for each modality at different decoding steps, (ii) decomposes them into language-representation and language-control roles, and (iii) enables cross-modal comparison via overlap measures and causal intervention, including cross-modal steering of output language. Applying our framework to SeamlessM4T v2, we find that cross-modal language alignment is strongest at the first decoding step, where language-representation neurons are shared across modalities, but weakens as generation proceeds, indicating a shift toward modality-specific autoregressive processing. In contrast, language-control neurons identified from speech transfer causally to text generation, revealing partially shared circuitry for output-language control that strengthens at later decoding steps. These results show that cross-modal processing is both time- and function-dependent, providing a more nuanced view of multilingual computation in speech–text models.

Code: <https://github.com/konta3738/generation-step-aware-framework>

1 Introduction

Multilingual speech–text foundation models aim to unify tasks such as automatic speech recognition, speech translation, and text translation within a single architecture that processes both spoken and written language (Cheng et al., 2023; Rubenstein et al., 2023; Tang et al., 2024a). A central premise behind such models is *cross-modal language alignment*: representations associated with the same language should remain sufficiently compatible across speech and text for multilingual knowledge to transfer across modalities. If this alignment is weak, models may rely on modality-specific computation even for the same language, limiting generalization.

Despite its importance, it remains unclear whether the same circuitry is reused to represent or output the same language across different modalities, and how. Prior mechanistic interpretability work on multilingual *text-only* models identifies language-selective neurons which react specifically to certain languages, finding that those are concentrated in early and late layers, with mid-layers being language-agnostic (Kojima et al., 2024; Tang et al., 2024b; Tan et al., 2024; Gurgurov et al., 2025; Trinley et al., 2025). However, comparable neuron-level evidence for *multimodal* models remains scarce. In particular, we lack a clear account of whether multilingual speech–text models have language-selective neurons that react to both speech and text inputs, or instead rely on modality-specific processing, without shared mechanism for the same language.

A key limitation of existing neuron-based methods (Cuadros et al., 2022; Kojima et al., 2024) is that they collect decoder activations under full-sequence conditioning, rather than the

prefix available at each decoding step. This mismatches the autoregressive computation, where predictions are conditioned only on previously generated tokens and therefore vary across steps. In encoder-decoder speech models, early decoding relies primarily on encoder-derived representations, whereas later steps increasingly depend on target-side context (Reid, 2023). This issue is particularly important in multilingual speech–text models, where encoder representations carry modality-specific information.

In this work, we revisit cross-modal language alignment through the lens of *functional decomposition*. We ask: *how and when do multilingual speech–text models reuse shared circuitry across modalities, and how does this reuse differ between input-language representation and output-language generation during decoding?* To answer this, we introduce a generation-step-aware diagnostic framework, which extends prior Average Precision (AP) based neuron identification for text models (Cuadros et al., 2022; Kojima et al., 2024) in three key ways: it (i) identifies language-selective neurons separately for each modality at different decoding steps, (ii) decomposes them by functional role, and (iii) enables direct cross-modal comparison through overlap- and rank-based measures, as well as causal intervention. This unified framework enables systematic evaluation of when, how, and to what extent language processing is shared across modalities. We demonstrate the applicability of our framework through a detailed case study on SeamlessM4T v2 (Communication et al., 2023), whose shared decoder provides a suitable testbed for cross-modal evaluation.

We decompose decoder-side language processing into two functionally distinct components. *Language-representation neurons* capture how the input language is internally encoded when the output language is fixed, while *language-control neurons* capture mechanisms involved in determining which language is generated. This decomposition enables us to study cross-modal language alignment not as a single property, but as a function of the role that language plays in the computation.

Applying our framework to SeamlessM4T v2, we reveal two forms of cross-modal language alignment on the input and output sides.

(i) **Input-side (representation-level alignment)**. At the first decoding step, language-representation neurons are strongly shared across modalities for the same language, indicating cross-modal language alignment at the representation level. However, this overlap decreases as generation proceeds (56.6% \rightarrow \sim 35%), suggesting a transition toward modality-specific autoregressive processing.

(ii) **Output-side (control-level alignment)**. Language-control neurons identified from speech also influence output language in text generation, indicating that output-language control relies on partially shared neuron-level mechanisms across modalities. This cross-modal alignment in control becomes stronger at later decoding steps, with the mean cross-modal effect ratio increasing from 0.36 at $t = 6$ to 0.49 at $t = 11$.

Our contributions are threefold. First, we introduce **generation-step-aware framework**, which models neuron specialization as a function of decoding step and enables cross-modal evaluation of multilingual speech–text models. Second, we show that multilingual representations in a shared decoder exhibit **strong temporal structure**, transitioning from shared cross-modal computation at early decoding steps to more modality-specific autoregressive processing. Third, we provide, to the best of our knowledge, **the first causal evidence of cross-modal steering** at the neuron level, showing that language-control neurons identified from speech transfer to text generation and can be used to change the output language.

2 Related work

2.1 Language-selective neurons in text-only models

Prior work identifies language-selective neurons using activation statistics or information-theoretic measures (Cuadros et al., 2022; Tang et al., 2024b; Tan et al., 2024; Gurgurov et al., 2025), some of which can be used for output-language control. AP-based ranking (Kojima et al., 2024) selects neurons that best discriminate languages at the full sentence level, ignoring the autoregressive nature of decoding. Tan et al. (2024) instead identify

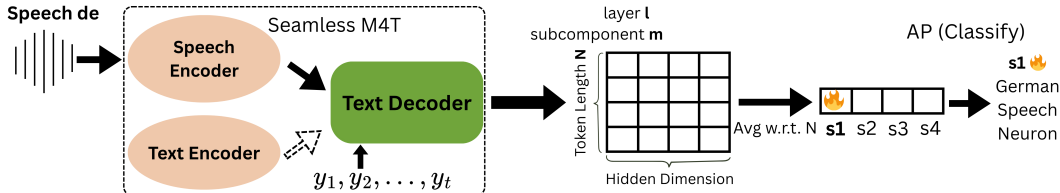


Figure 1: Overview of generation-step-aware neuron identification (length adapter omitted). For each decoding step $t \in 1, 6, 11$, we collect activations and identify language-specific neurons via Average Precision (AP) ranking (Cuadros et al., 2022; Kojima et al., 2024), which are further categorized into *language-representation* and *language-control* neurons.

neurons based on activation frequency in encoder–decoder models, but treat the decoder as effectively static by conditioning on the first decoding step (i.e., BOS token). Existing work is limited to text-only models. Our framework builds on these approaches by explicitly modeling neuron specialization as a function of decoding steps and conditioning context.

2.2 Mechanistic interpretability in speech–text models

Mechanistic interpretability for speech and speech–text models remains relatively limited. Prior work on Whisper (Radford et al., 2023) shows that the encoder primarily captures acoustic structure while the decoder acts as a conditional language model (Reid, 2023). Other studies analyze cross-attention contributions (Papi et al., 2025) and cross-lingual similarity, finding weaker alignment in speech than in text representations (Lee et al., 2025). Despite these advances, neuron-level evaluations of multilingual speech–text models are scarce, motivating our study.

3 Model and method

This section introduces the experimental setup and diagnostic framework used to study cross-modal processing in multilingual speech–text models. We first describe the SeamlessM4T v2 (Communication et al., 2023) architecture and the submodules analyzed in this work. Next, we present the datasets and tasks used to define language-representation and language-control settings. Finally, we introduce our generation-step-aware diagnostic framework.

3.1 Model and submodules

We study SeamlessM4T v2 Large, which consists of a Conformer-based speech encoder, (w2v-BERT 2.0, Communication et al., 2023), a Transformer-based text encoder in the style of NLLB, and a shared Transformer text decoder (Costa-jussà et al., 2024). Each module has 24 layers (0–23). For speech generation, the decoder’s text representations are further processed by additional components (e.g., speech-specific encoders/decoders and a vocoder) to synthesize audio. Since the shared text decoder is the point at which representations from different modalities are unified, we restrict our targets to text outputs and do not examine the speech-generation pathway. We investigate all submodules that expose a hidden (neuron) dimension, including attention, feed-forward, layer normalization, and convolutional components (Appendix A.1 for details).

3.2 Data and tasks

We use the FLEURS benchmark (Conneau et al., 2023), a multilingual parallel speech dataset. In this work, we employ FLEURS for four tasks: speech-to-text (S2T) translation, and text-to-text (T2T) translation ($X \rightarrow \text{En}$), automatic speech recognition (ASR), and text repetition.

To control for acoustic variability, we synthesize speech from the FLEURS transcriptions using XTTS v2 (Casanova et al., 2024). This yields 1,000 utterances per language across five

languages (German/de, Spanish/es, French/fr, Mandarin/zh, and Japanese/ja). Using single-speaker synthetic speech removes confounds related to speaker identity and recording conditions, allowing us to focus on model-internal representations.

3.3 Generation-step-aware diagnostic framework

We introduce our three-step framework for systematically evaluating cross-modal computation: (i) generation-step-aware neuron identification, (ii) cross-modal comparison, and (iii) cross-modal steering.

(i) Generation-step-aware neuron identification. Our goal is to model neuron specialization as a function of decoding steps and conditioning context, capturing its dynamic nature during autoregressive generation (Figure 1). In this step, language-selective neurons are identified separately for each modality.

Neuron definition and pooling. Following prior work (Cuadros et al., 2022; Tan et al., 2024; Tang et al., 2024b; Kojima et al., 2024), we define a *neuron* as a single hidden dimension j of an intermediate activation. Let $X_{\text{enc}} = (x_1, \dots, x_n)$ denote the encoder input and $X_{\text{dec},t} = (y_1, \dots, y_t)$ the decoder prefix available at generation step t . For layer l and submodule m , let $\mathbf{A}_{\text{enc}}^{(l,m)}(X_{\text{enc}}) \in \mathbb{R}^{n \times d}$ and $\mathbf{A}_{\text{dec}}^{(l,m)}(X_{\text{dec},t} | X_{\text{enc}}) \in \mathbb{R}^{t \times d}$ denote encoder and decoder activations.

For encoder-side modules, we obtain one scalar score per neuron by mean-pooling over the sequence dimension:

$$[\mathbf{s}_{\text{enc}}^{(l,m)}(X_{\text{enc}})]_j = \frac{1}{n} \sum_{i=1}^n [\mathbf{A}_{\text{enc}}^{(l,m)}(X_{\text{enc}})]_{i,j}.$$

For decoder-side modules, in contrast, we define neuron activity at generation step t using the activation at the current decoding position:

$$[\mathbf{s}_{\text{dec}}^{(l,m)}(X_{\text{dec},t} | X_{\text{enc}})]_j = [\mathbf{A}_{\text{dec}}^{(l,m)}(X_{\text{dec},t} | X_{\text{enc}})]_{t,j}.$$

This asymmetric definition matches the model’s computation: encoder representations are distributed over the full input sequence, equivalent with the formulation of prior work on decoder-only models (Cuadros et al., 2022; Kojima et al., 2024), whereas decoder representations are generated autoregressively and are therefore indexed by decoding step.

Average-precision ranking. For each layer–submodule pair (l, m) and each decoding condition, we rank neurons by how well their pooled activations discriminate a target language. Let $\mathcal{D} = \{X_{\text{enc},i}, X_{\text{dec},t}\}_{i=1}^p$ be a dataset with binary labels $z_i \in \{0, 1\}$ indicating membership in a target language class. For neuron j , we collect its pooled activations across examples and compute $\text{AP}_j^{(l,m)} = \text{AP}(\mathbf{s}_j^{(l,m)}, \mathbf{z})$, where higher AP indicates that the neuron more reliably distinguishes the target language. Following Kojima et al. (2024), we select both **top- k** neurons (highest AP) and **bottom- k** neurons (lowest AP), corresponding to excitatory and inhibitory associations with the target language.

Label construction. We construct binary labels according to the specialization type of interest. In this work, we use **unimodal language labels**: language classification is performed separately within each modality (speech-only or text-only), so that neuron rankings reflect language distinctions *within* a modality rather than modality differences themselves. This design enables later cross-modal comparison between independently identified language-selective neuron sets.

Types of specialized neurons. Having defined how neurons are identified and labeled, we now define two types of language-selective neurons according to the task used to collect activations.

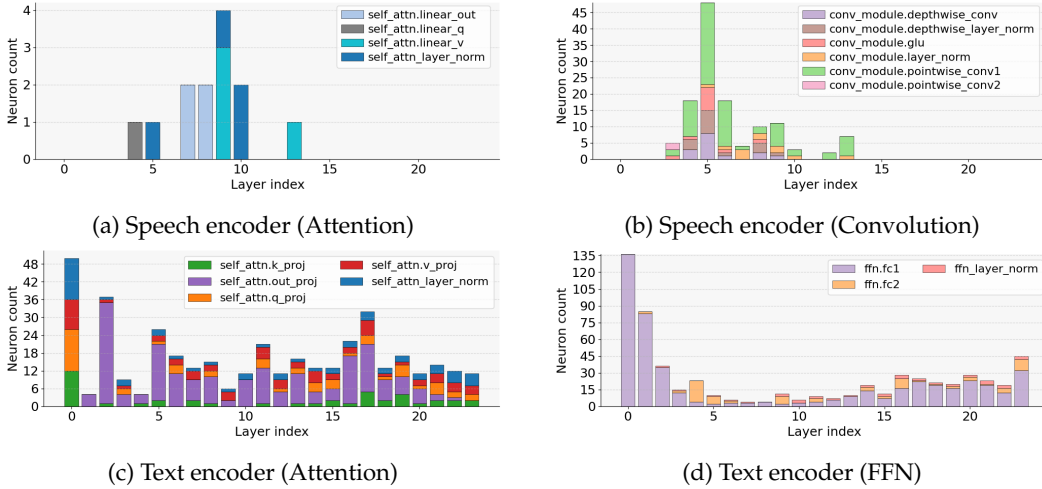


Figure 2: Layer-wise distribution of top-1,000 language-representation neurons. In the speech encoder, neurons concentrate in middle layers, whereas in the text encoder they peak at the first layer, reflecting that language information must be extracted from continuous acoustic input in speech but is already explicit in discrete text tokens.

1. **Language-representation neurons.** These are identified from speech-to-text translation (S2T) and text-to-text translation (T2T) in the $X \rightarrow \text{En}$ setting. Because the output language is fixed to English while the input language varies, these neurons are intended to capture how input language is internally represented across modalities. In the main analysis, we focus on top-k neurons, as they correspond to the most strongly language-selective units and provide a clearer basis for cross-modal overlap comparison.
2. **Language-control neurons.** These are identified from automatic speech recognition (ASR), where the output language varies together with the input. They are therefore intended to capture mechanisms involved in output-language generation and control. For this intervention, we consider both top-k and bottom-k neurons, since both excitatory and inhibitory associations can influence output-language generation under intervention.

We perform identification separately at three decoding steps: $t = 1$, $t = 6$, and $t = 11$. The first step corresponds to generation of the first token, while later steps reflect decoding after target-side context has begun to accumulate.

(ii) **Cross-modal comparison.** To quantify cross-modal language alignment, we compare neuron sets identified independently from speech and text under matched decoder conditions. For each decoding step, let A_i denote the top-k neuron set identified from speech for language i , and B_j the corresponding top-k neuron set identified from text for language j , with $k = 1000$. We construct an overlap matrix M with entries $M_{ij} = |A_i \cap B_j|$.

To measure same-language alignment across modalities, we define the *diagonal overlap ratio* as

$$\text{DiagOverlap}(M) = \frac{\sum_i M_{ii}}{\sum_{i,j} M_{ij}}.$$

A high diagonal overlap ratio indicates that overlap is concentrated on same-language speech-text pairs, whereas a low ratio indicates that overlap is more diffusely distributed across different-language pairs. To complement the set-based evaluation, we also compute Spearman correlation between neuron-wise AP scores across modalities over the full set of neurons (Appendix A.3).

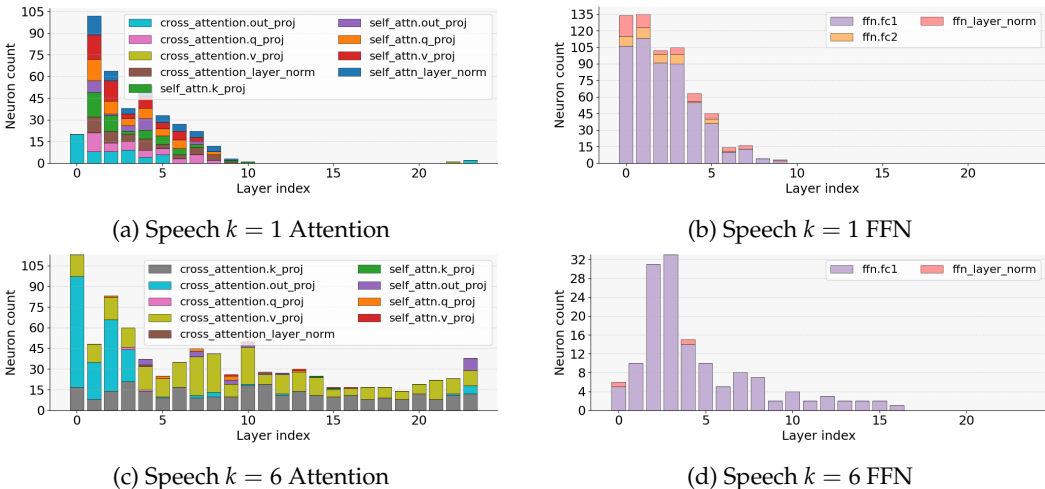


Figure 3: Distribution of top-1,000 language-representation neurons in the decoder across decoding steps (from German speech). Language selectivity shifts from self-attention at $t = 1$ to cross-attention at $t = 6$, indicating a transition from encoder-driven to autoregressive processing.

(iii) Cross-modal steering. To test whether identified neurons are causally involved in output-language generation, we perform median-value interventions during inference, following (Kojima et al., 2024). Specifically, we replace the activations of targeted neurons with their median values estimated from corresponding activation distributions.

We apply this intervention to top&bottom-1000 **language-control neurons** identified from ASR and evaluate whether they also shift the output language in a different modality, namely text repetition. This cross-modal transfer design allows us to test whether output-language control circuitry is shared across speech and text.

We quantify output-language switching using token-level script classification (Latin vs. CJK) with regular expressions. Unlike sentence-level language identification tools such as fastText (Joulin et al., 2017), which assume a single dominant label and are unreliable for code-mixed outputs, this provides a simple and robust proxy. We report the *control rate*, defined as the proportion of tokens matching the target script, and use it to assess cross-modal transfer.

We define the *cross-modal effect ratio* as $\text{ControlRate}_B / \text{ControlRate}_A$, where A denotes the source modality used for neuron identification (ASR) and B the target modality (text). This metric quantifies how strongly language-control effects transfer across modalities (details in Appendix A.5).

4 Step-dependent cross-modal language Representations

4.1 Distribution of language neurons

Having established the cross-modal evaluation framework, we next examine how language-representation neurons are distributed across the speech encoder, text encoder, and shared decoder. For each module and decoder step, we report the distributions of top-1,000 neurons identified from German speech and German text, respectively.

Speech encoder. Figures 2(a) and (b) show that language-representation neurons concentrate in middle layers (approximately 4–10), indicating that language-dependent processing emerges after initial acoustic processing and becomes more abstract in later layers.

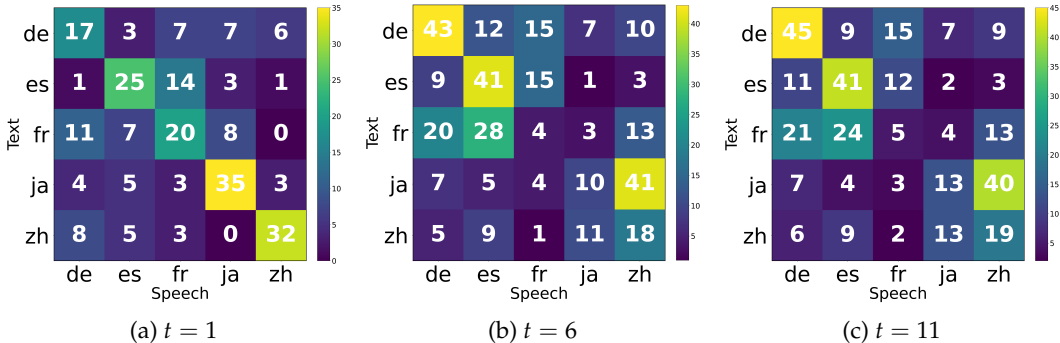


Figure 4: Cross-modal neuron overlap between speech and text in the decoder. Same-language overlap is strongest at $t = 1$ (diagonal structure) and weakens at later steps, indicating that shared representations diminish as autoregressive context accumulates.

We also observe component-level skew, where certain pointwise convolutional submodules contain more language-selective neurons than expected, while attention sublayers contribute comparatively fewer.

Text encoder. Figures 2(c) and (d) show that language-representation neurons peak in the first layer, indicating that language identity is primarily captured by surface-form cues such as script and lexical statistics. Unlike speech, text does not involve speaker or prosodic variation, making early-layer features highly diagnostic of language identity.

Text decoder. Figures 3 show that language selectivity shifts from self-attention at $t = 1$ (a) to cross-attention at $t = 6$ (c), indicating a transition from encoder-driven processing to autoregressive, context-dependent computation.

At $t = 1$, language selectivity is concentrated primarily in self-attention (query, key, value, and layer normalization), whereas at $t = 6$, it shifts predominantly to cross-attention (key, value, and output projections). This pattern suggests that early decoding relies more heavily on encoder-derived representations, while later steps increasingly depend on autoregressive target-side context. These results indicate that the focus of language processing in the decoder is strongly position-dependent, rather than fixed across generation.

4.2 Cross-modal neuron overlap

To examine how cross-modal language alignment evolves during decoding, we compare the overlap between language-representation neurons identified from speech and text.

Figure 4 shows that same-language overlap is strongest at $t = 1$ and weakens at later steps, indicating that shared cross-modal representations are most prominent at the onset of decoding but diminish as autoregressive context accumulates while cross-language overlaps (e.g., French–Spanish, Japanese–Chinese) becoming more prominent.

Quantitatively, the diagonal overlap ratio is highest at $t = 1$ (56.6%) and decreases at later steps (34.63% at $t = 6$, 36.83% at $t = 11$). Notably, while the diagonal preference weakens, the overall amount of overlap in absolute terms increases at later decoding steps, suggesting that representations become less language-specific but more entangled across modalities as autoregressive context accumulates.

An exact permutation test over language matchings confirms that this diagonal preference exceeds chance at all steps ($t = 1$: $p = 0.0083$; $t = 6$: $p = 0.0417$; $t = 11$: $p = 0.0417$), with the strongest effect at $t = 1$.

These results indicate that cross-modal language alignment is strongest at the initial decoding step but becomes progressively less structured as generation proceeds, reflecting a

Task lang	Task	Intervention	t=1		t=6		t=11	
			Latin	CJK	Latin	CJK	Latin	CJK
German	ASR	Japanese	100.00	0.00	39.15	60.85	16.68	83.32
German	ASR	Chinese	100.00	0.00	25.04	74.96	14.19	85.81
German	TR	Japanese	100.00	0.00	85.84	14.16	77.11	22.89
German	TR	Chinese	100.00	0.00	83.25	16.75	68.33	31.67
French	ASR	Japanese	100.00	0.00	34.66	65.34	13.24	86.76
French	ASR	Chinese	100.00	0.00	22.27	77.73	10.51	89.49
French	TR	Japanese	100.00	0.00	89.66	10.34	74.04	25.96
French	TR	Chinese	100.00	0.00	69.30	30.70	49.15	50.85
Japanese	ASR	German	0.10	99.90	89.28	10.72	95.43	4.57
Japanese	ASR	French	0.10	99.90	33.64	66.36	43.78	56.22
Japanese	TR	German	0.55	99.45	63.12	36.88	77.08	22.92
Japanese	TR	French	0.59	99.41	11.48	88.52	24.03	75.97
Chinese	ASR	German	0.55	99.45	91.69	8.31	95.58	4.42
Chinese	ASR	French	0.61	99.39	51.43	48.57	71.60	28.40
Chinese	TR	German	1.89	98.11	50.47	49.53	58.96	41.04
Chinese	TR	French	2.19	97.81	15.09	84.91	31.15	68.85

Table 1: Script distribution (%) under language-control neuron interventions. Effective control emerges only at later decoding steps ($t = 6, t = 11$), with substantial script shifts and cross-modal transfer, while $t = 1$ shows minimal effect. Control rate for each task language is highlighted in bold.

shift from shared, language-specific representations toward more entangled cross-modal processing.

5 Cross-modal steering

5.1 Language control results

To evaluate whether language-control neurons causally influence output language, we examine script changes under intervention across decoding steps.

Table 1 shows that effective language control emerges only at later decoding steps, with substantial script shifts observed at $t = 6$ and $t = 11$, while $t = 1$ exhibits minimal control.

At $t = 1$, interventions show little evidence of effective control from German/French to Chinese/Japanese, as outputs remain entirely in Latin script. In the reverse direction, interpretation is less reliable due to natural mixing of Latin characters in CJK outputs.

At $t = 6$, interventions become substantially more effective. In ASR, German/French \rightarrow Chinese/Japanese conversions yield over 50% CJK script, while the reverse direction reaches up to 91.69% Latin. Importantly, these effects transfer across modalities: applying ASR-derived neurons to text repetition still shifts the output script (10.34%–63.12%).

At $t = 11$, this trend further strengthens. For example, Chinese ASR controlled toward German reaches 95.58% Latin script. Consistently, the mean cross-modal ratio of language control increases from 0.36 at $t = 6$ to 0.49 at $t = 11$, indicating improved cross-modal transfer at later decoding steps. This trend is consistently observed across language pairs that satisfy the source-modality threshold.

Overall, these results show that language-control neurons identified at later generation steps are more causally involved in output-language generation. In contrast, neurons identified at $t = 1$ likely reflect initial language-tag signals rather than mechanisms that govern subsequent generation.

Condition	Output
Gold	in entwickelten ländern werden sie selten ähnlich viele beschwerden über die wasserqualität oder den einsturz von brücken hören
ASR	在发达的国家,你会你很少类似许多投诉关于水质或桥梁的崩塌的听
Text repetition	in entwickelten Ländern werden sie很少类似地许多 Beschwerden über die水质 oder den einsturz von brücken

Table 2: Example of German-to-Chinese intervention with neurons identified from ASR. The intervention shifts the output toward Chinese in ASR and induces mixed-language output in text repetition.

5.2 Qualitative evaluation

To qualitatively assess the effect of steering, we examine representative outputs under cross-modal transfer.

Table 2 shows that the steered output preserves semantic content while changing the output language, providing qualitative evidence that complements the limitations of the script-based metric. We also observe that source-language syntax is largely preserved. Additional examples are provided in Appendix A.7.

6 Discussion

Input-side: step-dependent cross-modal similarity. We observe a clear temporal pattern in cross-modal similarity of language-representation neurons. Similarity is highest *in relative terms* at the first decoding step ($t = 1$), despite a smaller absolute number of overlapping neurons, and decreases substantially as generation proceeds.

We attribute this pattern to the shift in available information during decoding. At $t = 1$, the model must rely entirely on encoder-derived representations, without autoregressive context. Under this constraint, language information is processed in a more modality-agnostic manner, resulting in higher relative overlap across modalities.

As generation proceeds, previously generated tokens provide strong language cues. The model can therefore rely on autoregressive context, reducing the need for shared neuron-level representations across modalities. This leads to more modality-specific trajectories and a decrease in fine-grained overlap. Importantly, this does not imply that shared structure disappears: higher-level organization (e.g., typological structure) remains stable across decoding steps.

Output-side: partially shared control mechanisms. In contrast, language-control neurons exhibit a different pattern. Steering using neurons identified at later decoding steps ($t = 6$, $t = 11$) are more effective than those at $t = 1$, and transfer from ASR to text generation. This provides causal evidence that output-language control relies on partially shared mechanisms across modalities.

Moreover, the cross-modal effect ratio increases at later decoding steps, indicating that neurons identified under richer autoregressive context generalize more strongly across modalities. Our interpretation is that, as context accumulates, next-token prediction in the decoder becomes more dominant, allowing control signals to operate in a more modality-independent manner.

7 Conclusion

We revisited cross-modal alignment in multilingual speech-text models through a generation-step-aware diagnostic framework. We showed that cross-modal similarity in language representations is highest at the first decoding step and decreases substantially

as generation proceeds (56.6% \rightarrow \sim 35%), indicating a shift from shared, modality-agnostic computation to more modality-specific autoregressive processing.

In contrast, language-control neurons transfer causally from speech to text, providing evidence for partially shared output-language control mechanisms. This cross-modal transfer becomes stronger at later decoding steps, with the mean effect ratio increasing from 0.36 at $t = 6$ to 0.49 at $t = 11$.

Overall, our results show that cross-modal processing is both *time-dependent* and *function-dependent*, highlighting the importance of generation-aware diagnostics for evaluating multilingual behavior in multimodal models.

8 Limitations

Our study has several limitations.

First, we focus on a single model architecture. SeamlessM4T v2 is currently the only publicly available multilingual speech–text model with a shared decoder that enables controlled neuron-level comparison across modalities. While this limits empirical coverage, our findings may extend to other sequence-to-sequence multimodal models.

Second, our framework relies on AP-based neuron identification, which captures statistical associations between neuron activations and linguistic labels but does not establish causal necessity. Although we complement this with intervention experiments, our conclusions remain constrained by this framework.

Third, we use synthetic speech to control for acoustic variability. While this improves comparability, future work should verify whether similar patterns hold for natural speech.

Finally, our evaluation setup introduces asymmetries across tasks. In particular, language tags in ASR and text repetition might introduce some noise in the neuron identification step, and ASR and text repetition differ in their linguistic objectives, which may affect neuron identification and cross-modal comparisons. More symmetric settings, such as $En \rightarrow X$ translation across modalities, should be explored in future work.

Acknowledgments

We thank Yifan Wang for helpful feedbacks.

Ethics Statement

This work evaluates internal processing mechanisms of a multilingual speech–text model via activation recording and neuron-level interventions. It does not involve human subjects, user interaction, or deployment in real-world decision-making systems.

We use publicly available resources, namely SeamlessM4T v2 and the FLEURS dataset, in accordance with their respective licenses. Speech inputs are generated via text-to-speech synthesis using XTTS v2 conditioned on a single speaker. The synthesized audio does not contain real personal data, and we do not reveal or infer any identifying information about individuals.

References

- Edresson Casanova, Kelly Davis, Eren Gölge, Görkem Gökner, Iulian Gulea, Logan Hart, Aya Aljafari, Joshua Meyer, Reuben Morais, Samuel Olayemi, and Julian Weber. XTTS: a Massively Multilingual Zero-Shot Text-to-Speech Model. In *Interspeech 2024*, pp. 4978–4982, 2024. doi: 10.21437/Interspeech.2024-2016.
- Yong Cheng, Yu Zhang, Melvin Johnson, Wolfgang Macherey, and Ankur Bapna. Mu²SLAM: Multitask, multilingual speech and language models. In Andreas Krause, Emma Brun-

- skill, Kyunghyun Cho, Barbara Engelhardt, Sivan Sabato, and Jonathan Scarlett (eds.), *Proceedings of the 40th International Conference on Machine Learning*, volume 202 of *Proceedings of Machine Learning Research*, pp. 5504–5520. PMLR, 23–29 Jul 2023. URL <https://proceedings.mlr.press/v202/cheng23e.html>.
- Seamless Communication, Loïc Barrault, Yu-An Chung, Mariano Coria Meglioli, David Dale, Ning Dong, Mark Duppenthaler, Paul-Ambroise Duquenne, Brian Ellis, Hady Elsahar, Justin Haaheim, John Hoffman, Min-Jae Hwang, Hirofumi Inaguma, Christopher Klaiber, Iliia Kulikov, Pengwei Li, Daniel Licht, Jean Maillard, Ruslan Mavlyutov, Alice Rakotoarison, Kaushik Ram Sadagopan, Abinеш Ramakrishnan, Tuan Tran, Guillaume Wenzek, Yilin Yang, Ethan Ye, Ivan Evtimov, Pierre Fernandez, Cynthia Gao, Prangthip Hansanti, Elahe Kalbassi, Amanda Kallet, Artyom Kozhevnikov, Gabriel Mejia Gonzalez, Robin San Roman, Christophe Touret, Corinne Wong, Carleigh Wood, Bokai Yu, Pierre Andrews, Can Balioglu, Peng-Jen Chen, Marta R. Costa-jussà, Maha Elbayad, Hongyu Gong, Francisco Guzmán, Kevin Heffernan, Somya Jain, Justine Kao, Ann Lee, Xutai Ma, Alex Mourachko, Benjamin Pelloquin, Juan Pino, Sravya Popuri, Christophe Ropers, Safiyyah Saleem, Holger Schwenk, Anna Sun, Paden Tomasello, Changhan Wang, Jeff Wang, Skyler Wang, and Mary Williamson. Seamless: Multilingual expressive and streaming speech translation, 2023. URL <https://arxiv.org/abs/2312.05187>.
- Alexis Conneau, Min Ma, Simran Khanuja, Yu Zhang, Vera Axelrod, Siddharth Dalmia, Jason Riesa, Clara Rivera, and Ankur Bapna. Fleurs: Few-shot learning evaluation of universal representations of speech. In *2022 IEEE Spoken Language Technology Workshop (SLT)*, pp. 798–805, 2023. doi: 10.1109/SLT54892.2023.10023141.
- Marta R. Costa-jussà, James Cross, Onur Çelebi, Maha Elbayad, Kenneth Heafield, Kevin Heffernan, Elahe Kalbassi, Janice Lam, Daniel Licht, Jean Maillard, Anna Sun, Skyler Wang, Guillaume Wenzek, Al Youngblood, Bapi Akula, Loïc Barrault, Gabriel Mejia Gonzalez, Prangthip Hansanti, John Hoffman, Semarley Jarrett, Kaushik Ram Sadagopan, Dirk Rowe, Shannon Spruit, Chau Tran, Pierre Andrews, Necip Fazil Ayan, Shruti Bhosale, Sergey Edunov, Angela Fan, Cynthia Gao, Vedanuj Goswami, Francisco Guzmán, Philipp Koehn, Alexandre Mourachko, Christophe Ropers, Safiyyah Saleem, Holger Schwenk, Jeff Wang, and NLLB Team. Scaling neural machine translation to 200 languages. *Nature*, 630(8018):841–846, June 2024. ISSN 1476-4687. doi: 10.1038/s41586-024-07335-x. URL <https://doi.org/10.1038/s41586-024-07335-x>.
- Xavier Suau Cuadros, Luca Zappella, and Nicholas Apostoloff. Self-conditioning pre-trained language models. In Kamalika Chaudhuri, Stefanie Jegelka, Le Song, Csaba Szepesvari, Gang Niu, and Sivan Sabato (eds.), *Proceedings of the 39th International Conference on Machine Learning*, volume 162 of *Proceedings of Machine Learning Research*, pp. 4455–4473. PMLR, 17–23 Jul 2022. URL <https://proceedings.mlr.press/v162/cuadros22a.html>.
- Daniil Gurgurov, Katharina Trinley, Yusser Al Ghussin, Tanja Baeumel, Josef Van Genabith, and Simon Ostermann. Language arithmetics: Towards systematic language neuron identification and manipulation. In Kentaro Inui, Sakriani Sakti, Haofen Wang, Derek F. Wong, Pushpak Bhattacharyya, Biplab Banerjee, Asif Ekbal, Tanmoy Chakraborty, and Dharendra Pratap Singh (eds.), *Proceedings of the 14th International Joint Conference on Natural Language Processing and the 4th Conference of the Asia-Pacific Chapter of the Association for Computational Linguistics*, pp. 2911–2937, Mumbai, India, December 2025. The Asian Federation of Natural Language Processing and The Association for Computational Linguistics. ISBN 979-8-89176-298-5. URL <https://aclanthology.org/2025.ijcnlp-long.156/>.
- Armand Joulin, Edouard Grave, Piotr Bojanowski, and Tomas Mikolov. Bag of tricks for efficient text classification. In Mirella Lapata, Phil Blunsom, and Alexander Koller (eds.), *Proceedings of the 15th Conference of the European Chapter of the Association for Computational Linguistics: Volume 2, Short Papers*, pp. 427–431, Valencia, Spain, April 2017. Association for Computational Linguistics. URL <https://aclanthology.org/E17-2068/>.
- Takeshi Kojima, Itsuki Okimura, Yusuke Iwasawa, Hitomi Yanaka, and Yutaka Matsuo. On the multilingual ability of decoder-based pre-trained language models: Finding and

- controlling language-specific neurons. In Kevin Duh, Helena Gomez, and Steven Bethard (eds.), *Proceedings of the 2024 Conference of the North American Chapter of the Association for Computational Linguistics: Human Language Technologies (Volume 1: Long Papers)*, pp. 6919–6971, Mexico City, Mexico, June 2024. Association for Computational Linguistics. doi: 10.18653/v1/2024.naacl-long.384. URL <https://aclanthology.org/2024.naacl-long.384/>.
- Hyunji Lee, Danni Liu, Supriti Sinhamahapatra, and Jan Niehues. How do multi-modal foundation models encode text and speech? an analysis of cross-lingual and cross-modal representations. In Luis Chiruzzo, Alan Ritter, and Lu Wang (eds.), *Proceedings of the 2025 Conference of the Nations of the Americas Chapter of the Association for Computational Linguistics: Human Language Technologies (Volume 2: Short Papers)*, pp. 600–610, Albuquerque, New Mexico, April 2025. Association for Computational Linguistics. ISBN 979-8-89176-190-2. doi: 10.18653/v1/2025.naacl-short.51. URL <https://aclanthology.org/2025.naacl-short.51/>.
- Sara Papi, Dennis Fucci, Marco Gaido, Matteo Negri, and Luisa Bentivogli. Cross-attention is half explanation in speech-to-text models, 2025. URL <https://arxiv.org/abs/2509.18010>.
- Alec Radford, Jong Wook Kim, Tao Xu, Greg Brockman, Christine Mcleavey, and Ilya Sutskever. Robust speech recognition via large-scale weak supervision. In Andreas Krause, Emma Brunskill, Kyunghyun Cho, Barbara Engelhardt, Sivan Sabato, and Jonathan Scarlett (eds.), *Proceedings of the 40th International Conference on Machine Learning*, volume 202 of *Proceedings of Machine Learning Research*, pp. 28492–28518. PMLR, 23–29 Jul 2023. URL <https://proceedings.mlr.press/v202/radford23a.html>.
- Ellena Reid. Interpreting openai’s whisper, 2023. URL <https://www.lesswrong.com/posts/thePw6qdyabD8XR4y/interpreting-openai-s-whisper>. Accessed: 2026-01-22.
- Paul K. Rubenstein, Chulayuth Asawaroengchai, Duc Dung Nguyen, Ankur Bapna, Zalán Borsos, Félix de Chaumont Quitry, Peter Chen, Dalia El Badawy, Wei Han, Eugene Kharitonov, Hannah Muckenhirn, Dirk Padfield, James Qin, Danny Rozenberg, Tara Sainath, Johan Schalkwyk, Matt Sharifi, Michelle Tadmor Ramanovich, Marco Tagliasacchi, Alexandru Tudor, Mihajlo Velimirović, Damien Vincent, Jiahui Yu, Yongqiang Wang, Vicky Zayats, Neil Zeghidour, Yu Zhang, Zhishuai Zhang, Lukas Zilka, and Christian Frank. Audiopalm: A large language model that can speak and listen, 2023. URL <https://arxiv.org/abs/2306.12925>.
- Shaomu Tan, Di Wu, and Christof Monz. Neuron specialization: Leveraging intrinsic task modularity for multilingual machine translation. In Yaser Al-Onaizan, Mohit Bansal, and Yun-Nung Chen (eds.), *Proceedings of the 2024 Conference on Empirical Methods in Natural Language Processing*, pp. 6506–6527, Miami, Florida, USA, November 2024. Association for Computational Linguistics. doi: 10.18653/v1/2024.emnlp-main.374. URL <https://aclanthology.org/2024.emnlp-main.374/>.
- Changli Tang, Wenyi Yu, Guangzhi Sun, Xianzhao Chen, Tian Tan, Wei Li, Lu Lu, Zejun Ma, and Chao Zhang. SALMONN: Towards generic hearing abilities for large language models. In *The Twelfth International Conference on Learning Representations*, Vienna, Austria, May 2024a. OpenReview.net. URL <https://openreview.net/forum?id=14rn7HpKVk>.
- Tianyi Tang, Wenyang Luo, Haoyang Huang, Dongdong Zhang, Xiaolei Wang, Xin Zhao, Furu Wei, and Ji-Rong Wen. Language-specific neurons: The key to multilingual capabilities in large language models. In Lun-Wei Ku, Andre Martins, and Vivek Srikumar (eds.), *Proceedings of the 62nd Annual Meeting of the Association for Computational Linguistics (Volume 1: Long Papers)*, pp. 5701–5715, Bangkok, Thailand, August 2024b. Association for Computational Linguistics. doi: 10.18653/v1/2024.acl-long.309. URL <https://aclanthology.org/2024.acl-long.309/>.
- Katharina A. T. T. Trinley, Toshiki Nakai, Tatiana Anikina, and Tanja Baeumel. What language(s) does aya-23 think in? how multilinguality affects internal language representations. In Sudhansu Bala Das, Pruthwik Mishra, Alok Singh, Shamsuddeen Hassan Muhammad, Asif Ekbal, and Uday Kumar Das (eds.), *Proceedings of the Workshop on Beyond*

English: *Natural Language Processing for all Languages in an Era of Large Language Models*, pp. 159–171, Varna, Bulgaria, September 2025. INCOMA Ltd., Shoumen, BULGARIA. URL <https://aclanthology.org/2025.globalnlp-1.18/>.

A Appendix

We present additional details and results which complement our main text.

A.1 Parametrization of model components

Table 5 reports the parameter counts of SeamlessM4T v2 Large used in our experiments, providing context for our module-wise analyses and evaluations. In our intervention experiments, when we replace 2,000 neurons, it corresponds to only 0.44% of the decoder parameters.

We exclude attention distance-embedding activations from our neuron identification step, which lack a neuron dimension and are therefore excluded.

A.2 Synthesized audio quality

As described in Subsection 3.2, we re-synthesized the FLEURS utterances using a text-to-speech (TTS) model. For all six languages (English, German, Spanish, French, Japanese, and Mandarin), we manually inspected the generated audio. For five languages, the speech was natural and fully intelligible. For Mandarin, the audio was generally understandable but occasionally exhibited pronunciation errors.

Illustrative example. The following Mandarin sentence from FLEURS is shown in pinyin only (Chinese characters omitted for clarity):

Target sentence (pinyin):

Hàn Mì'ěrdùn quèrèn Huò Huá Dé dàxué yīyuàn shōuzhì de bìngrén qíngkuàng wěndìng.

Gloss:

Hamilton confirm Howard University hospital admit-DE patient condition stable.

Intended meaning:

“Hamilton confirmed that the condition of the patients admitted by Howard University Hospital was stable.”

Observed synthesis errors. The synthesized speech deviates from the target pronunciation in several ways. **Phoneme substitution:** *quèrèn* → *kuèrèn*, introducing an illicit onset in Mandarin. **Word-boundary errors:** *bìngrén qíngkuàng* (“patient condition”) → *bìngrénqíng kuàng*. **Syllable insertion:** *de* → *dede*, *wěndìng* → *wěndìnggua*.

Impact on evaluation. Although these errors indicate limitations in synthetic Mandarin speech, they do not affect sentence-level intelligibility and occur only sporadically. Since our study focuses on cross-lingual and cross-modal representational patterns rather than fine-grained phonetic accuracy, we expect their impact on the reported results to be minimal.

A.3 Spearman correlation evaluation

To assess global cross-modal similarity beyond top-ranked neurons, we compute Spearman correlations over the full set of neuron activations.

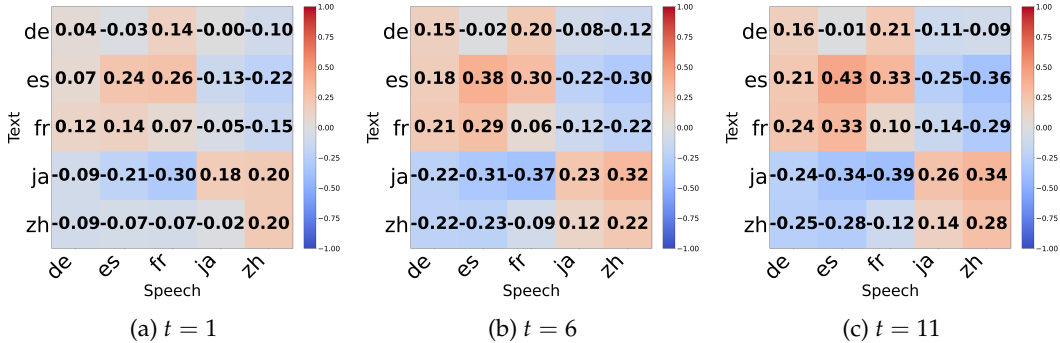


Figure 5: Spearman correlation between speech- and text-conditioned neuron activations in the decoder. Correlation patterns remain stable across decoding steps and reflect typological clustering rather than same-language alignment, while fine-grained overlap has strict same language alignment at $t = 1$.

Figure 5 shows that correlation patterns remain stable across decoding steps and reflect typological clustering rather than strict same-language alignment, indicating that global ranking captures coarse-grained cross-modal structure.

This contrasts with the overlap evaluation, where same-language alignment weakens at later steps, revealing a divergence between fine-grained and global representations.

Across all decoding steps, languages cluster into typological groups (e.g., French, Spanish, and German vs. Japanese and Chinese), rather than exhibiting strict same-language alignment.

To quantify this, we measure the proportion of correlation mass concentrated on the diagonal:

$$\frac{\sum_i |\rho_{ii}|}{\sum_{i,j} |\rho_{ij}|} \tag{1}$$

where ρ_{ij} denotes the Spearman correlation between conditions i and j .

We find that diagonal concentration remains stable across decoding steps (22.9% at $t = 1$, 20.1% at $t = 6$, and 20.9% at $t = 11$), confirming that same-language correspondence is weak at the global level and does not exhibit strong step dependence (but equally strongest at $t = 1$ as in the fine-grained neuron overlap measure).

Taken together, these results indicate that multilingual speech–text models maintain stable, typology-driven global structure.

A.4 Sensitivity to k in overlap evaluation

To assess the robustness of our results to the choice of k , we analyze the diagonal ratio of the cross-modal overlap matrix across different values of k .

Figure 6 shows that same-language overlap is consistently highest at the first decoding step ($t = 1$) across all choices of k , confirming that our main finding is robust to the number of selected neurons.

As generation proceeds, the overlap decreases at $t = 6$ and partially recovers at $t = 11$ (except for $k = 100$, where the recovery is less pronounced).

These results suggest that strong cross-modal alignment at early decoding steps is driven by a relatively small subset of highly specialized neurons. As decoding progresses, this alignment weakens, reflecting a shift toward more distributed and context-dependent processing.

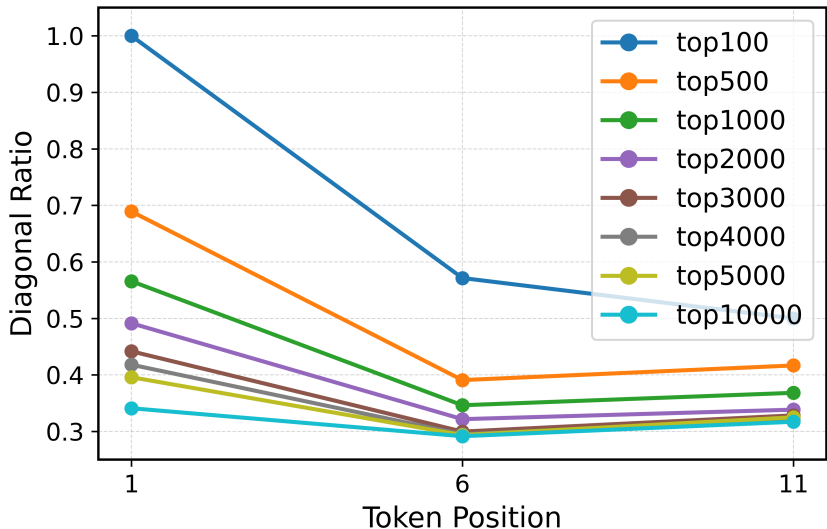


Figure 6: Sensitivity of cross-modal overlap to the choice of k . We report the diagonal ratio of the overlap matrix (i.e., proportion of same-language overlap) across decoding steps. Across all values of k , the overlap is highest at $t = 1$, decreases at $t = 6$, and partially recovers at $t = 11$ (except for $k = 100$). This indicates that our findings are robust to k , and that a relatively small subset of neurons exhibits strong cross-modal alignment at early decoding steps.

Task	Intervention	t	ASR	TR	Ratio
$t = 6$					
Chinese	French	6	51.43	15.09	0.29
Chinese	German	6	91.69	50.47	0.55
French	Chinese	6	77.73	30.70	0.39
French	Japanese	6	65.34	10.34	0.16
German	Chinese	6	74.96	16.75	0.22
German	Japanese	6	60.85	14.16	0.23
Japanese	French	6	33.64	11.48	0.34
Japanese	German	6	89.28	63.12	0.71
$t = 11$					
Chinese	French	11	71.60	31.15	0.44
Chinese	German	11	95.58	58.96	0.62
French	Chinese	11	89.49	50.85	0.57
French	Japanese	11	86.76	25.96	0.30
German	Chinese	11	85.81	31.67	0.37
German	Japanese	11	83.32	22.89	0.27
Japanese	French	11	43.78	24.03	0.55
Japanese	German	11	95.43	77.08	0.81

Table 3: Cross-modal effect ratios for all language pairs satisfying $\text{ControlRate}_A > \tau$. Ratios increase at later decoding steps, indicating stronger cross-modal transfer.

A.5 Cross-modal effect ratio

We report the *cross-modal effect ratio* defined in Section 3, computed as $\text{ControlRate}_B / \text{ControlRate}_A$, where A denotes the source modality (ASR) and B the target modality (text repetition). This ratio quantifies how strongly language-control effects identified in one modality transfer to another.

Task lang	Task	Intervention	t=1		t=6		t=11	
			src	tgt	src	tgt	src	tgt
German	ASR	Japanese	99.06	0.01	39.63	40.22	8.42	70.88
German	ASR	Chinese	99.07	0.00	24.25	52.07	3.12	73.29
German	TR	Japanese	99.09	0.00	92.81	5.42	83.75	11.86
German	TR	Chinese	99.10	0.00	93.27	4.69	84.44	11.04
French	ASR	Japanese	98.72	0.01	37.28	22.14	11.20	39.75
French	ASR	Chinese	98.73	0.00	20.09	41.94	6.62	58.17
French	TR	Japanese	98.60	0.01	94.21	1.66	81.10	12.41
French	TR	Chinese	98.74	0.01	82.32	13.24	63.13	29.57
Japanese	ASR	German	99.97	0.00	15.44	60.18	5.28	72.91
Japanese	ASR	French	99.97	0.00	84.34	9.37	74.87	14.29
Japanese	TR	German	99.99	0.00	44.90	39.89	25.47	54.31
Japanese	TR	French	98.99	0.00	95.38	2.87	84.50	6.67
Chinese	ASR	German	97.52	0.08	8.80	69.30	1.46	74.73
Chinese	ASR	French	95.67	0.46	52.74	38.05	35.96	54.35
Chinese	TR	German	99.11	0.00	63.69	32.26	55.08	38.54
Chinese	TR	French	99.10	0.00	91.47	7.51	82.16	15.83

Table 4: FastText-based evaluation of language control under neuron interventions. Target-language probabilities increase substantially at later decoding steps ($t = 6$, $t = 11$), confirming that language control becomes effective over time and supporting the script-based results with an independent metric. Target-language probabilities are highlighted in bold.

To ensure reliability, we only compute ratios for cases with $\text{ControlRate}_A > \tau$, where $\tau = 0.1$, excluding cases where control in the source modality is too weak to yield meaningful comparisons.

Table 3 reports cross-modal effect ratios for all valid language pairs. We find that the ratio consistently increases from $t = 6$ to $t = 11$, indicating that cross-modal transfer of language-control effects becomes stronger as generation proceeds.

While variability exists across language pairs, this trend is consistent and not driven by a small number of outliers.

A.6 FastText-based language control evaluation

To validate our script-based evaluation with an independent metric, we measure language probabilities using fastText.

Table 4 shows that target-language probabilities increase substantially at later decoding steps, confirming that language control becomes effective over time.

At $t = 1$, the probability assigned to the target language remains close to zero across all conditions, indicating minimal language shift. At later decoding steps ($t = 6$ and $t = 11$), the target language probability increases substantially, and in some cases exceeds that of the source language (e.g., German→Chinese in ASR at $t = 6$, and Japanese→German in text repetition at $t = 11$).

These results are consistent with the script-based metric and provide complementary evidence that output-language control strengthens at later decoding steps. The fact that the same neurons induce similar shifts in both ASR and text repetition further suggests that output-language control partially relies on shared circuitry across modalities.

A.7 Qualitative evaluation on language control

Interestingly, in the ASR example (Table 2), the output shifts to Chinese lexical items while partially preserving German word order. In particular, in the gold German sentence, the verb *hören* (‘hear’) appears at the end of the clause because it is governed by the auxiliary verb

werden ('will'). While in Chinese the verb 听 ('hear') would normally be placed following the auxiliary verb 会 ('will'), the model placed 听 ('hear') at the end of the sentence, partially preserving German syntax.

To complement the qualitative evaluation in the main text, we present additional qualitative examples. We manually looked into all the examples to confirm that the intervention changes the output language, and not only the script. All examples shown here are taken from $t = 11$. Across these cases, the intervention often changes lexical language identity, but does not reliably impose well-formed target-language syntax.

Example 2: Japanese → German intervention.

Gold: 寺院の一部としてジグラットと呼ばれるピラミッド型の特殊な塔が建てられる
 ことがありました
ASR: 寺院の一部としてZikrと呼ばれるpyramidalforms spezialn tower gebet gebet
 gebet gebet gebet gebet ...
Text repetition: 寺院の一部としてジグラットと呼ばれるPilaamid-Types特殊なTaarが
 erbaetされることがありました。

The intervention yields unstable outputs. In ASR, decoding collapses into repetition, while in text repetition, several items are shifted toward German-like forms but remain malformed, such as *Taar* instead of *Turm* and *erbaet* instead of *erbaut*. This suggests that the intervention biases lexical language identity, but is insufficient to ensure correct word forms or coherent syntax.

Example 3: German → Chinese intervention.

Gold: zeit ist auch die art und weise wie wir die dauer länge von veranstaltungen
 vergleichen
ASR: 时间 ist也theart和方式,怎么我们比较活动的持续时间
Text repetition: zeit ist auch die 艺术和方式 wie wir die dauer länge von veranstaltun-
 gen比较

The outputs show mixed-language sequences and inconsistent word order. For example, *vergleichen* is mapped to 比较, but its position differs across ASR and text repetition. The outputs also contain lexical distortions such as *theart* and the contextually inappropriate translation 艺术. This suggests that the intervention affects lexical language identity without deterministically controlling syntax.

Example 4: Chinese → French intervention.

Gold: 11 点20 分警察要求抗议者退回到人行道并告知抗议者在行使抗议权利时务必考
 虑到越来越拥堵的公共交通问题
ASR: onze heures vingt police demande les protestants de revenir à la rue des gens et
 d'invoquer les protestants de se réveiller les protestants de se réveiller les protestants
 de se réveiller ...
Text repetition: 11 点20 分警察要求抗议者退回到人行道并告知抗议者 En 行使抗议权
 利时务必考虑 En 越 venir 越拥堵的公共交通问题

The ASR output begins with plausible French material, such as *onze heures vingt*, but soon degenerates into repetition. In text repetition, most of the sentence remains in Chinese, with isolated French insertions. Notably, part of the fixed expression 越来越 is translated as *venir*, suggesting that the model translates subcomponents of a construction rather than preserving the construction as a unit. This again shows that the intervention affects lexical language identity more strongly than higher-level structural planning.

Summary. Across Examples 2–5, the intervention consistently influences lexical language identity, but does not reliably enforce target-language syntax. The outputs often preserve source-language structure, produce malformed target-language forms, or become unstable

during decoding. These cases therefore support our interpretation that the identified language neurons contribute to output-language control, but are not sufficient to account for full syntactic planning.

A.8 Additional implementation details

Speech preprocessing. All speech inputs are resampled to 16 kHz. Log-mel filterbank features are extracted with $n_{\text{mels}} = 160$, and a fixed temporal length of $T = 300$ is enforced via truncation or zero-padding.

Subcomponents. For Conformer components with activations of shape $d \times n$, we consistently treat the hidden dimension d as the neuron axis.

We exclude attention distance-embedding activations from our experiment, as they do not possess a neuron (hidden) dimension.

Module	Submodule	Component	Neurons (dim)	
Speech encoder	FFN	ffn1_layer_norm	1024	
		ffn1.intermediate_dense	4096	
		ffn1.output_dense	1024	
		ffn2_layer_norm	1024	
		ffn2.intermediate_dense	4096	
		ffn2.output_dense	1024	
	Attention	layer_norm	1024	
		linear_q	1024	
		linear_k	1024	
		linear_v	1024	
		linear_out	1024	
	Convolution	conv_module.layer_norm	1024	
		conv_module.pointwise_conv1	2048	
		conv_module.glu	1024	
		conv_module.depthwise_conv	1024	
conv_module.depthwise_layer_norm		1024		
conv_module.pointwise_conv2		1024		
Total neurons per layer			24 576	
Total across 24 layers			589 824 (0.33%)	
Text encoder	Attention	self_attn.layer_norm	1024	
		self_attn.q_proj	1024	
		self_attn.k_proj	1024	
		self_attn.v_proj	1024	
		self_attn.out_proj	1024	
	FFN	ffn_layer_norm	1024	
		ffn.fc1	8192	
		ffn.fc2	1024	
	Total neurons per layer			15 360
	Total across 24 layers			368 640 (0.54%)
Text decoder	Self-attention	self_attn.layer_norm	1024	
		self_attn.q_proj	1024	
		self_attn.k_proj	1024	
		self_attn.v_proj	1024	
		self_attn.out_proj	1024	
	Cross-attention	cross_attn.layer_norm	1024	
		cross_attn.q_proj	1024	
		cross_attn.k_proj	1024	
		cross_attn.v_proj	1024	
		cross_attn.out_proj	1024	
	FFN	ffn_layer_norm	1024	
		ffn.fc1	8192	
		ffn.fc2	1024	
Total neurons per layer			20 480	
Total across 24 layers			491 520 (0.40%)	

Table 5: Activation dimensionalities (“neurons”) for each component in SeamlessM4T v2. Component names follow implementation conventions; e.g., `self_attn.q_proj` corresponds to the query projection in self-attention. Percentages denote the fraction covered by the selected 2,000 neurons per module.